Effect of NO upon N_2O Decomposition over Fe/ZSM-5 with Low Iron Loading†

Chimin Sang, Bryan H. Kim, and Carl R. F. Lund*

Department of Chemical and Biological Engineering, University at Buffalo, SUNY, Buffalo, New York 14260-4200

Received: March 12, 2004; In Final Form: July 12, 2004

An Fe/ZSM-5 catalyst with a very high Si/Al ratio was prepared, and using it, the effect of NO upon the kinetics of N_2O decomposition was studied. The addition of small, nonstoichiometric amounts of NO was observed to cause the rate to increase by more than an order of magnitude. The kinetics were well-fit by a rate expression that was first order in the partial pressure of N_2O for the situation without added NO and separately for the situation where NO was added. The Arrhenius parameters of the rate coefficient differed for the two situations. The results are consistent with a mechanistic scheme wherein the reaction proceeds via an oxide−oxo redox cycle in the absence of NO. The results suggest that the NO-assisted decomposition of N_2O does not require a second iron site adjacent to the active site and that NO_x species adsorbed on the same cation site could serve as locations for oxygen storage if, in fact, the promotional effect of NO is related to such storage.

Introduction

The oxidation−reduction properties of iron cations exchanged into zeolites have been know for some time,[1,2] and zeolites that contain ion-exchanged iron are now know to be catalytically active for several reduction−oxidation (redox)-type reactions.[3−7] One such reaction is the decomposition of N_2O.[5,8−15] It has been observed that the addition of small, substoichiometric amounts of NO causes the rate of N_2O decomposition to increase significantly.[12,15] The kinetics of the N_2O decomposition reaction, with and without added NO, have been studied on samples of Fe/ZSM-5 where the loading of iron is relatively large.[15] On the basis of these studies, it has been suggested[15] that NO adsorbs on nonactive iron sites that are adjacent to active iron sites. It has then been further suggested that this adsorbed NO can be converted to adsorbed NO_2 which can more readily supply an oxygen atom back to the active iron sites than it can be supplied by gas phase N_2O. In this way, the rate-limiting catalyst reduction step is replaced with a step that involves oxygen stored in an NO_2 species adsorbed on an iron site adjacent to the active iron site.[15]

In the work presented here, Fe/ZSM-5 has been prepared using a form of the zeolite that has a very high Si/Al ratio and, correspondingly, a very low ion exchange capacity. The very high Si/Al ratio leads to a catalyst where most of the catalytically active iron is believed to exist as isolated ion-exchanged ferric cations that have no other iron species in close proximity. The research reported here was undertaken to determine whether such catalysts would still show an increased rate of N_2O decomposition when small, substoichiometric amounts of NO were added.

Experimental Section

An Fe/ZSM-5 catalyst was prepared from an ammonium-exchanged form of the zeolite procured from Zeolyst International (CBV 28014). The as-supplied material was first heated in a muffle furnace to 393 K and held at this temperature for 2 h (to eliminate moisture), after which it was heated at 1 K/min to 873 K and held at this temperature for 18 h. This treatment is expected to decompose the ammonium cations and convert the zeolite to the hydrogen-exchanged form. A method analogous to that described by Chen and Sachtler[16−23] was used to introduce ion-exchanged iron. This method has been described previously.[12,24] Briefly, stainless steel tubing was packed with iron chloride (upstream) and H/ZSM-5 (downstream), and the contents were dried in flowing He at 553 K for 1 h. The temperature was then increased to 578 K, whereupon the iron chloride began to sublime, as evidenced by its eventual condensation in the outlet tubing. After some time, the exhaust tubing became blocked at which point the helium flow was shut off and the temperature was reduced to ambient. The resulting zeolite sample displayed a uniform yellow color. It was subsequently rinsed repeatedly with deionized, distilled water. The rinsed material was then dried under vacuum, ground, and calcined overnight in air at 1073 K.

The apparent N_2 BET surface area (before and after iron loading) and the total adsorptive NO uptake of the catalyst were measured volumetrically. X-ray diffraction patterns were recorded using a Siemens D-500 X-ray diffractometer with Cu Kα radiation. The patterns were recorded over a 2θ range from 5° to 40° at a rate of 0.02° s^{-1}. Chemical composition analysis was performed by Galbraith Laboratories using inductively coupled plasma optical emission spectroscopy.

N_2O decomposition kinetics were studied in a quartz tubular reactor operating at atmospheric pressure. N_2O (Matheson, UHP) and NO (Matheson, CP grade) were used without further purification; He (Cryogenic Supply, high-purity grade) was purified using a gas drying tube, a Supelco carrier gas purifier, and a Supelco OMI-2 indicating purifier. The tubular reactor was positioned along the vertical axis of a tube furnace. One K-type thermocouple was positioned immediately under the catalyst bed and the quartz wool that supported it; a second K-type thermocouple was situated so it just touched the upper

† Part of the special issue "Michel Boudart Festschrift".

* Corresponding author. Phone: (716) 645-2911. Fax: (716) 645-3822. E-mail: lund@eng.buffalo.edu.

10.1021/jp048884m CCC: $30.25
Published on Web 08/24/2004

surface of the catalyst bed. The reaction temperature used for the kinetic analysis was taken as equal to the reading from this upper thermocouple. The maximum difference between the two readings in any experiment was 13 K; normally the difference was considerably smaller than this. The reactor temperature was controlled using a computer. Gas flows to the top of the reactor were controlled using a VICI SA202 flow controller for N_2O and Omega FMA 760 mass flow controllers for the other gases. The compositions of the gases leaving the reactor were analyzed using a Varian 1400 gas chromatograph (GC) with Haysep D and 5A molecular sieve columns and a thermal conductivity detector. A gas sampling valve (Valco) was used to inject samples onto the GC column. The detector signal was collected and integrated using PeakSimple II software (SRI).

The kinetic runs were performed by first establishing a stable reactor temperature with only helium flowing through the reactor. A series of measurements was then made wherein the total outlet flow rate was held constant, but the ratio of N_2O to He in the feed was varied. In any one series, the temperature and the inlet flow rate of NO were held constant. After each change in the N_2O/He ratio, the outlet composition was analyzed until it appeared to have reached a steady level, then the N_2O/He ratio was readjusted. The outlet flow rate was measured using a bubble flow meter.

The only gases used in the feed in these experiments were He, N_2O, and NO. For experimental series where NO was not added to the feed, the data were first checked to make sure that the product N_2/O_2 ratio was equal to the stoichiometrically expected value of 2.0. Specifically, if the measured N_2/O_2 ratio was not between 1.9 and 2.1, it was assumed that the reactor had not yet reached steady state, and that data point was not used in the kinetic analysis. When NO was present in the feed, data were used only if the stoichiometry was similarly satisfied. In either case (with or without added NO) the kinetic analysis did not use any data where the N_2O decomposition reaction had gone to completion.

The kinetic modeling was performed using Athena Visual Workbench.[25] The reactor was modeled as a steady-state, isothermal plug-flow reactor, and the N_2O decomposition kinetics were assumed to be first order in the partial pressure of N_2O. In those cases where NO was added, the amount was typically equal to ca. 5% of the N_2O in the feed, and as shown later, its stoichiometric reaction with N_2O would lead to a small change in the N_2O concentration compared to that caused by direct N_2O decomposition. The analytical instrumentation did not permit sufficiently accurate quantification of the small amounts of NO_x components produced to permit modeling of this reaction separately. However, since the total N_2O conversion due to this reaction is small and since the reaction of NO with O_2 to produce NO_2 is very rapid, even at room temperature, it was deemed acceptable to use a worst-case analysis wherein complete conversion of NO was assumed and only the N_2O conversion above and beyond that was attributed to direct N_2O decomposition and kinetically modeled as such. Accordingly, when NO was present in the feed it was assumed that all of the NO reacted immediately according to reaction 1 leading to a set of effective inlet molar flow rates, ($\dot{n}_i^{in}$), which were calculated from the actual experimental feed molar flow rates ($\dot{n}_i^0$) using equations 2−6. These effective inlet molar flow rates were then used as the initial conditions for solving the reactor mole balance equations 7−11. In the latter equations, $\dot{n}_i$ denotes the molar flow rate of species i, m denotes the catalyst mass, k_0 is the apparent first-order Arrhenius preexponential factor for direct N_2O decomposition, E is the corresponding activation energy for direct N_2O decomposition, R is the gas constant, T is the temperature, and P is the total pressure. In Athena, initial guesses were provided for k_0 and E. For each experimental data point, Athena then used equations 2−11 to calculate predicted outlet flow rates for that experimental point. These in turn were used to calculate the predicted effluent mole fraction of O_2. The values of k_0 and E were then adjusted within Athena so as to minimize the sum of the squares of the differences between the predicted and measured effluent O_2 mole fractions. Thus, with Athena it was possible to analyze data for all temperatures simultaneously. However, as discussed later, it proved necessary to analyze experiments wherein NO was added to the feed separately from experiments where NO was not added.

$$N_2O + NO \rightarrow NO_2 + N_2 \tag{1}$$

$$\dot{n}_{N_2O}^{in} = \dot{n}_{N_2O}^0 - \dot{n}_{NO}^0 \tag{2}$$

$$\dot{n}_{N_2}^{in} = \dot{n}_{N_2}^0 + \dot{n}_{NO}^0 \tag{3}$$

$$\dot{n}_{O_2}^{in} = \dot{n}_{O_2}^0 \tag{4}$$

$$\dot{n}_{NO_2}^{in} = \dot{n}_{NO}^0 \tag{5}$$

$$\dot{n}_{He}^{in} = \dot{n}_{He}^0 \tag{6}$$

$$\frac{d\dot{n}_{N_2O}}{dm} = -2k_0 \exp\left(\frac{-E}{RT}\right)P_{N_2O} = -2k_0 \exp\left(\frac{-E}{RT}\right)\frac{\dot{n}_{N_2O}P}{(\dot{n}_{N_2O} + \dot{n}_{N_2} + \dot{n}_{O_2} + \dot{n}_{NO_2} + \dot{n}_{He})} \tag{7}$$

$$\frac{d\dot{n}_{N_2}}{dm} = 2k_0 \exp\left(\frac{-E}{RT}\right)\frac{\dot{n}_{N_2O}P}{(\dot{n}_{N_2O} + \dot{n}_{N_2} + \dot{n}_{O_2} + \dot{n}_{NO_2} + \dot{n}_{He})} \tag{8}$$

$$\frac{d\dot{n}_{O_2}}{dm} = k_0 \exp\left(\frac{-E}{RT}\right)\frac{\dot{n}_{N_2O}P}{(\dot{n}_{N_2O} + \dot{n}_{N_2} + \dot{n}_{O_2} + \dot{n}_{NO_2} + \dot{n}_{He})} \tag{9}$$

$$\frac{d\dot{n}_{NO_2}}{dm} = 0 \tag{10}$$

$$\frac{d\dot{n}_{He}}{dm} = 0 \tag{11}$$

The structure and energy of possible catalytic intermediate species were calculated using Jaguar, version 4.1.[26] Density functional theory (DFT) was employed using B3LYP hybrid exchange and correlation functionals. The LACVP** basis set was used; for the systems studied here, the LACVP** basis set is the same as the 6-31G** basis set except that it uses effective core potentials for the inner two electron shells of the iron atom (i.e., a Ne effective core). Fine DFT grids were employed, and ultrafine geometry convergence was specified. Symmetry constraints were not imposed upon any of the species investigated. Zero-point energies were not calculated, and corrections were not made for any possible basis set superposition errors. Mössbauer spectra obtained during some of the early experimental work on ion-exchanged iron in zeolites were interpreted in terms of high-spin ferrous and ferric species.[1,2] More recent studies have suggested that Fe^{4+} species might also be present.[27]

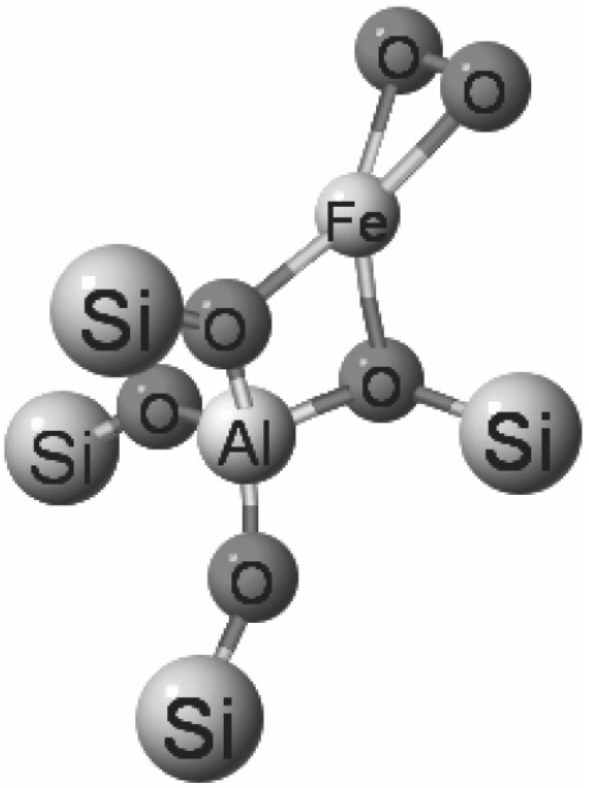

Figure 1. Computational cluster used to represent the active site in Fe/ZSM-5, here as an oxo species. Terminal hydrogen atoms that would be bonded to the silicon atoms are not shown.

Unfortunately, relatively few studies actually probe the oxidation state directly; more often it is inferred or assumed. The calculations presented here involve only iron in the ferric state. Generally, the iron has been assumed to exist in the high-spin form. In a few cases energies were calculated for different spin states, and in those cases the high-spin state was found to have the lowest energy.

A cluster model was used to represent the zeolite in these calculations. To generate the cluster, an Al atom was placed at the T1 position of the crystallographic structure of ZSM-5.[28] This Al atom, the four oxygen atoms bonded to it, and the four Si atoms bonded to those oxygen atoms were cut from the structure. The Si−O bonds that were broken in doing so were replaced with terminal Si−H bonds. A two step process was used to determine the length of the Si−H bonds. First, geometry optimization was performed with the spatial coordinates of the Si atoms held constant. The resulting Si−H bond lengths were all nearly equal, so the average value (1.48 Å) was selected. Returning to the original cluster, each Si−H bond was oriented to point in the same direction as the Si−O bond it was replacing but with the newly determined Si−H bond length. Ryder et al.[13] generated computational clusters in a very similar manner. Here, in all calculations on the cluster, the spatial coordinates of the terminal H atoms were held constant. In this way, the "real" atoms of the zeolite were free to move during geometry optimizations using different adsorbed species. Figure 1 shows the computational cluster for the case where an oxo species has formed on the ion-exchanged iron cation.

Results

The apparent BET surface area of the ZSM-5 catalyst was 427 $m^2\ g^{-1}$ before sublimation and 407 $m^2\ g^{-1}$ afterward. Chemical analysis by Galbraith Laboratories indicated a molar Si/Al ratio of 95 and an Fe/Al ratio of 2.59. The excess iron is believed to have existed as small particles of iron oxide which could be seen in the XRD patterns of the catalyst. These particles are not believed to have had a significant effect upon the kinetic phenomena studied since per iron cation Fe_2O_3 is reported to be several orders of magnitude less active than Fe/ZSM-5.[8] The active site density was taken to equal $3.68 \times 10^{19}\ g^{-1}$, equal to the amount of NO irreversibly adsorbed by the material. On the basis of the chemical analysis, this NO uptake corresponds to 0.4 NO/Al or 0.2 NO/Fe.

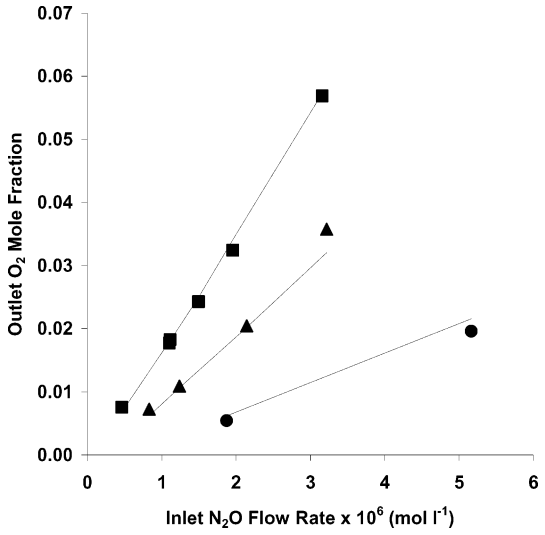

Figure 2. Comparison of experimental results (symbols) to first-order kinetic fit (lines) for N_2O decomposition at 785 K (squares), 760 K (triangles), and 736 K (circles) when NO is not added to the feed.

The location and the catalytic role of the iron in excess of the ion exchange capacity is very important for the work reported here. The XRD results show that iron oxide particles were present, and they were of sufficient size to generate a diffraction pattern. It may be noted that particles of such size likely would not fit within the narrow pores of ZSM-5 but instead would likely exist on the external surface of the ZSM-5 crystallites. In addition, one such crystallite would include many iron atoms. As an example, it can be estimated using the bulk density of iron oxide that a 25 Å (2.5 nm) iron oxide particle would contain ~323 iron atoms. On the basis of the analyzed composition of the catalyst (2.59 Fe per Al or 1.59 excess iron cations per exchanged iron cation) there would be one such particle for every ~203 ion-exchanged iron cations. Assuming a uniform distribution of ion exchange sites throughout the zeolite, such a particle might at most be in close proximity to two or three exchange cations. Thus, it is believed that the vast majority of the ion-exchanged iron exists as isolated species. As already noted, particles of iron oxide are several orders of magnitude less active in N_2O decomposition than iron cations in ZSM-5.[8]

In the absence of added NO, the kinetics of N_2O decomposition over Fe/ZSM-5 (and other iron-containing zeolites) are first order in N_2O and zero order in N_2 and O_2.[10,15] The data collected in this study were consistent with these reaction orders. Figure 2 presents kinetic data for three different temperatures, all obtained without the addition of NO. Simple first-order kinetics were fit to these data, and the corresponding predictions are also shown in the figure. It can be seen that the first-order fit was very good ($R^2 = 0.99$). The preexponential factor and activation energy associated with the first-order rate coefficient are presented in Table 1.

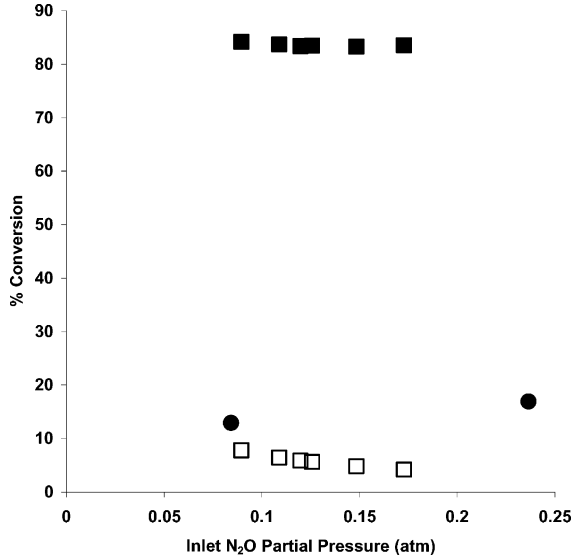

Figure 3. Conversion of N_2O at various inlet partial pressures without added NO (circles) and with 0.0067 atm NO present in the feed (squares). The filled squares show the total N_2O conversion; the unfilled squares show the maximum possible N_2O conversion via stoichiometric reaction with NO.

TABLE 1: Apparent Arrhenius Parameters for First-Order Kinetic Fits for N_2O Decomposition

P^0_{NO} atm	preexponential factor mol s^{-1} g^{-1} atm^{-1}	activation energy kJ mol^{-1}
0	3.18×10^9	194
0.0067	2.78×10^8	165

A number of additional experiments were performed wherein a small amount of NO was added to the feed. Figure 3 shows (as squares) the results of a representative experiment conducted at 738 K and 1 atm total pressure and with 0.0067 atm of NO in the feed. In the experiments shown, the partial pressure of N_2O was varied while holding the total pressure and total effluent flow rate constant. The figure shows (unfilled squares) that the complete conversion of all of the NO in the feed according to reaction 1 would consume less than 10% of the N_2O in the feed. Any additional conversion is then presumed to have occurred via N_2O decomposition. Figure 3 shows (as filled squares) that more than 80% of the N_2O present in the feed underwent decomposition. Figure 3 further shows that in similar experiments at comparable conditions, but that did not involve NO in the feed, less than ca. 20% of the feed N_2O decomposed. This jump at identical conditions other than inlet NO concentration, from 20% N_2O decomposition to 80% N_2O decomposition illustrates the promotional effect of NO upon the kinetics of N_2O decomposition. As mentioned, this effect has been studied in some detail using catalysts with higher iron loadings. The present results show that the effect persists in catalysts with very low iron content.

Three sets of experiments were performed, differing only in the partial pressure of NO in the reactor feed. Figure 4 shows the N_2O conversion due to decomposition for these experiments (i.e., it assumes sufficient additional N_2O was consumed to completely convert the added NO via reaction 1). It can be seen that the promotional effect of added NO reaches an asymptotic limit beyond which additional NO has no effect. A similar asymptotic behavior has been observed with a different Fe/ZSM-5 catalyst that had a lower Si/Al ratio and a higher Fe loading.[15]

In order to compare the kinetics of direct N_2O decomposition in the absence of added NO to those in the presence of added

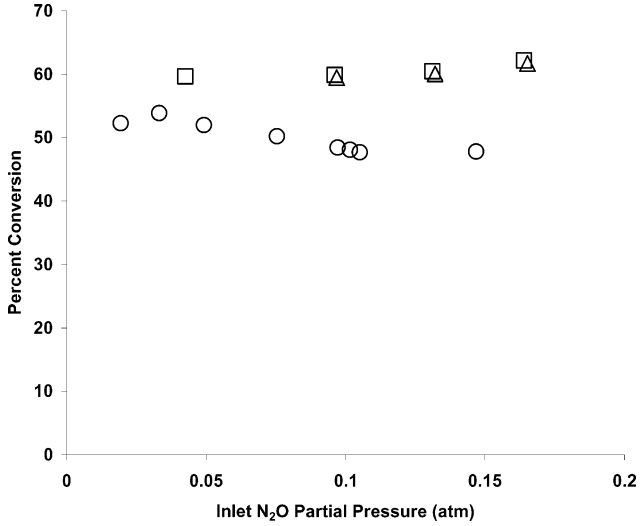

Figure 4. Observed N_2O conversion with varying partial pressures of NO in the feed: 0.006 atm (circles), 0.013 atm (squares), and 0.020 atm (triangles).

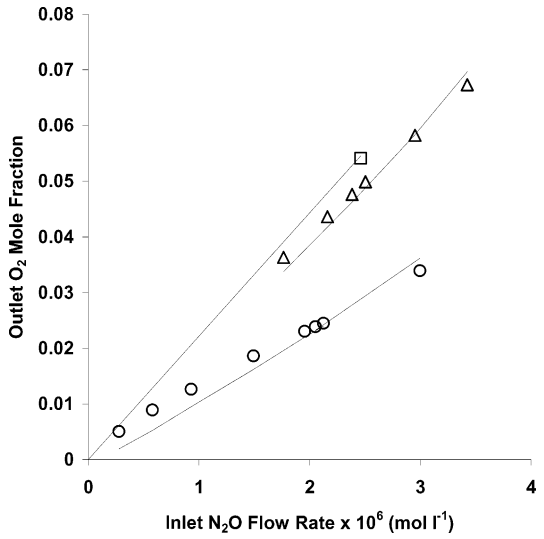

Figure 5. Comparison of experimental results (symbols) to first-order kinetic fit (lines) for N_2O decomposition at 763 K (squares), 739 K (triangles), and 710 K (circles) when NO is added to the feed at a partial pressure of 0.0067 atm.

NO, a simplifying assumption was made. Specifically, it was assumed that reaction 1 is extremely rapid compared to the N_2O decomposition reaction, as described in the Experimental Section. (If the added NO was not fully converted, this assumption would underestimate the conversion of N_2O due to direct decomposition, and so it is a conservative approximation.) The resulting mixture was then assumed to enter the packed bed reactor. First-order kinetics were fit to the data, and the results are plotted in Figure 5. As in Figure 2, the experimental results and the first-order predictions are compared, and again the fit can be seen to be very good ($R^2 = 0.99$). Thus, apparent first-order kinetics can describe the reaction both in the absence of added NO (Figure 2) and in its presence (Figure 5). The corresponding Arrhenius parameters are listed in Table 1. For comparison, Wood et al.[14] report an activation energy of 42 kcal/mol (176 kJ/mol) and Kapteijn et al.[10] report 168 kJ/mol.

Perez-Ramirez et al.[15] examined the effect of small amounts of NO upon the decomposition of N_2O over a variety of Fe-based catalysts including several Fe/ZSM-5 samples. All the studied materials had low Si/Al ratios, and therefore it might

SCHEME 1: Oxide−Oxo Redox Cycle

$$N_2O + \mathbf{FeO} \leftrightarrows N_2O\text{–}\mathbf{FeO} \quad (A)$$

$$N_2O\text{–}\mathbf{FeO} \leftrightarrows \mathbf{OFeO} + N_2 \quad (B)$$

$$N_2O + \mathbf{OFeO} \leftrightarrows N_2O\text{–}\mathbf{OFeO} \quad (C)$$

$$N_2O\text{–}\mathbf{OFeO} \leftrightarrows O_2\text{–}\mathbf{FeO} + N_2 \quad (D)$$

$$O_2\text{–}\mathbf{FeO} \leftrightarrows \mathbf{FeO} + O_2 \quad (E)$$

be expected that iron sites were present as pairs or ensembles with higher numbers of nearby iron neighbors. It was observed that the addition of substoichiometric amounts of NO caused a very large increase in the rate of N_2O decomposition over all the catalysts studied. The increase in activity was reflected in a decrease in the apparent activation energy by ca. 40−60 kJ mol^{-1}, and the effect was observed to attain an asymptotic limit above which additional NO had no effect. The results of the present study are in very good agreement with these results and show that systems where the majority of the iron cations are expected to be isolated behave in a manner similar to systems where the iron cations are expected to be in reasonably close proximity to each other. That is, the present results suggest that a nonactive iron site in close proximity to the active iron cations is not a necessity.

Discussion

From the time that the Boudart group[1,2] demonstrated that the ion-exchanged iron cations could be reversibly cycled between the ferrous and ferric states, catalytic redox reactions over ion-exchanged iron/zeolites were believed to take place via a cation redox mechanism. That is, the active site was thought to be an ion-exchanged iron cation that cycled between the ferrous and ferric states. Transient experiments wherein a sample initially containing ferrous cations was exposed to N_2O revealed that initially only N_2 was evolved until sufficient N_2O had been converted to oxidize the iron to the ferric state; after this, N_2 and O_2 were both evolved in stoichiometric amounts.[5,8] The kinetics were observed to be first order in N_2O and nearly zero order in both N_2 and O_2.[10] From the latter two observations it was inferred that the rate-limiting step in the reaction mechanism was the reduction of ferric cations to ferrous cations and that the most abundant surface intermediates were ferric cations. Kapteijn et al.[10] found that the addition of *stoichiometric* amounts of CO or NO increased the rate of N_2O decomposition over Fe/ZSM-5. The increase in reaction rate could be explained by the stoichiometric participation of either CO or NO so that the rate-determining catalyst reduction step was bypassed and thereby the overall rate increased (that is, the ferric cations were reduced by the added CO or NO and not by N_2O).

Later experiments yielded results that are more difficult to explain in terms of a cation redox mechanism.[5,12,15] For example,[5] when Fe/mordenite is exhaustively oxidized using labeled $^{18}O_2$ and then immediately used to catalyze the decomposition of $N_2{}^{16}O$, the initial product formed is $^{16}O_2$, not $^{18}O^{16}O$. Also, when the catalytic sites are predominantly isolated, then the redox cycling would need to involve Fe^{2+}/Fe^{4+} or Fe^{+}/Fe^{3+} instead of Fe^{2+}/Fe^{3+}. At present, the oxide−oxo mechanism shown here as Scheme 1 appears to be most consistent with available experimental and computational results[13,14] The present experimental results are consistent with Scheme 1, as can be seen by examination of Table 2. Specifically, Table 2 shows that first-order kinetics (as observed here) can result from Scheme 1 if any of the first four steps is rate-determining.

TABLE 2: Combinations of Rate-Limiting Steps (RDS) and Most Abundant Surface Intermediates (MASI) for Different Reaction Schemes Which Lead to a Rate Expression that Is First Order in N_2O and Zero Order in Other Species

scheme	RDS	MASI	rate expression
1, 2, 3	A	FeO	$k_A P_{N_2O}$
1, 2, 3	B	FeO	$k_B K_A P_{N_2O}$
1	C	OFeO	$k_C P_{N_2O}$
1	D	OFeO	$k_D K_C P_{N_2O}$
4	B	NO−FeO	$k_B P_{N_2O}$
4	C	NO−FeO	$k_C K_B P_{N_2O}$
4	D	NO_2−FeO	$k_D P_{N_2O}$
4	E	NO_2−FeO	$k_E K_D P_{N_2O}$
5	C	NO_2−FeO	$k_C P_{N_2O}$
5	D	NO−FeO	$k_D K_C P_{N_2O}$
5	E	NO_3−FeO	$k_E P_{N_2O}$
5	F	NO_3−FeO	$k_F K_E P_{N_2O}$

SCHEME 2: Oxide−Oxo Redox Cycle with Alternate Surface Catalyst Reduction

$$N_2O + \mathbf{FeO} \leftrightarrows N_2O\text{–}\mathbf{FeO} \quad (A)$$

$$N_2O\text{–}\mathbf{FeO} \leftrightarrows \mathbf{OFeO} + N_2 \quad (B)$$

$$NO + * \leftrightarrows NO\text{–}* \quad (C)$$

$$NO\text{–}* + \mathbf{OFeO} \leftrightarrows NO_2\text{–}* + \mathbf{FeO} \quad (D)$$

$$NO_2\text{–}* + \mathbf{OFeO} \leftrightarrows O_2\text{–}\mathbf{FeO} + NO\text{–}* \quad (E)$$

$$O_2\text{–}\mathbf{FeO} \leftrightarrows \mathbf{FeO} + O_2 \quad (F)$$

DFT calculations by Ryder et al.[13] indicate that step D in Scheme 1 is the rate-limiting step and that OFeO is the most abundant surface intermediate. It can be seen in Table 2 that these conditions will indeed lead to first-order kinetics as observed here. Table 2 further shows that the apparent rate constant under such circumstances will equal the product of the equilibrium constant for step C and the rate coefficient for step D. Correspondingly, the apparent activation energy will be equal to the sum of the true activation energy of step D and the enthalpy change for step C of Scheme 1. Ryder et al. calculated these two quantities separately finding the enthalpy change for step C to equal −23 kJ mol^{-1} and the activation barrier for step D to equal 187 kJ mol^{-1}, leading to an apparent activation energy of 164 kJ mol^{-1}, which agrees reasonably with experiment. While Scheme 1 represents the most likely pathway for N_2O decomposition it does not offer an explanation for the effect of adding substoichiometric amounts of NO.

Perez-Ramirez et al.[15] studied samples with higher iron loadings and suggested that added NO adsorbs on nonactive iron sites adjacent to the active iron sites. As shown in Scheme 2, they proposed that the adsorbed NO can accept an oxygen from an oxidized active site generating an adsorbed NO_2 and a reduced active site. Gas phase N_2O will readily reoxidize the reduced active site which can then be reduced by reaction with the adjacent NO_2. Recalling that step D of Scheme 1 is believed to be the rate-limiting step in the absence of NO, it can be seen that step E of Scheme 2 provides an alternative pathway that bypasses the rate-limiting step, and thereby Scheme 2 can explain the promotional effect of substoichiometric amounts of NO. Table 2 indicates that since the system still displays first-order kinetics when NO is added, then the most abundant surface intermediate would be expected to change from OFeO to FeO if Scheme 2 is operative. In the present investigation, however, the promotional effect of NO has been observed on samples where the iron cations are expected to be isolated. This observation necessitates a mechanistic explanation that does not involve extra sites adjacent to the catalytically active site, and

SCHEME 3: Oxide−Oxo Redox Cycle with Alternate Gas Phase Catalyst Reduction

$N_2O + \mathbf{FeO} \leftrightarrows N_2O\text{–}\mathbf{FeO}$ (A)

$N_2O\text{–}\mathbf{FeO} \leftrightarrows \mathbf{OFeO} + N_2$ (B)

$2\,NO + O_2 \leftrightarrows 2\,NO_2$ (C)

$NO_2 + \mathbf{OFeO} \leftrightarrows NO_2\text{–}\mathbf{OFeO}$ (D)

$NO_2\text{–}\mathbf{OFeO} \leftrightarrows O_2\text{–}\mathbf{FeO} + NO$ (E)

$O_2\text{–}\mathbf{FeO} \leftrightarrows \mathbf{FeO} + O_2$ (F)

hence, while Scheme 2 indicates a separate adsorption site (*), the present results indicate that it may instead just be a second ligand bonded to the active cation.

The work of Iglesia et al.[29−31] on Cu/ZSM-5 systems suggests another mechanistic possibility for the promotional effect of gas phase NO, shown here as Scheme 3. It is reasonable to expect that when NO is added, there will be rapid establishment of equilibrium with NO_2 according to reaction 12 or reaction 1. It would then be possible that gas phase NO/NO_2 (Scheme 3) could function in the same manner as proposed for surface NO/NO_2 in Scheme 2. Step E of Scheme 3 offers an alternative pathway, again bypassing the rate-limiting step D of the oxide−oxo pathway (Scheme 1). It can be seen in Table 2 that according to Scheme 3, first-order kinetics in N_2O will result if, as a result of bypassing the rate-limiting step, FeO again becomes the most abundant surface intermediate. This would agree with the present experimental results where the reaction is first order in N_2O both with added NO and without added NO.

$$2\,NO + O_2 \leftrightarrows 2\,NO_2 \qquad (12)$$

Schemes 2 and 3 are sufficiently similar in terms of the resulting reaction kinetics that they may be discussed simultaneously. Ryder et al.[13] calculated the activation energy of the rate-determining step in the absence of NO, step D of Scheme 1, to be 187 kJ mol^{-1}. As discussed above, this leads to an apparent first-order activation energy of 164 kJ mol^{-1}. They also found step A to be equilibrated ($\Delta H_A = -28$ kJ mol^{-1}), and they calculated an activation energy for step B of 157 kJ mol^{-1}. These results would suggest that if Scheme 3 is to explain the effect of adding NO, then step B of Scheme 3 must become the rate-determining step and, according to Table 2, the apparent rate coefficient should equal the product $k_B K_A$. This, in turn, would mean that the apparent activation energy should equal $\Delta H_A + E_B$ (129 kJ mol^{-1}). Thus, using the energies calculated by Ryder et al.,[13] the apparent activation energy would be expected to decrease by 35 kJ mol^{-1} (from 164 to 129) if Scheme 3 is to explain the observed effects of adding substoichiometric amounts of NO. Experimentally the observed change in apparent activation energy in the present work was 29 kJ mol^{-1} (from 194 to 165).

As just discussed, oxygen storage (via Scheme 2 or 3) offers a reasonable explanation for the effect of added NO, but it is not the only scheme to do so. Alternatively, it is possible that the addition of NO might open up entirely new pathways such as the nitrite−nitrate pathway originally proposed by Sang and Lund.[12] Schemes 4 and 5 are given here as two examples. The difference between the schemes, highlighted by boldface, is that the active site undergoes redox cycles between nitro and nitrite or between nitrite and nitrate. Table 2 shows that each is capable of giving first-order kinetics (consistent with experiment), and since the steps are entirely different, it is likely that the activation

SCHEME 4: Nitro−Nitrite Redox Cycle Replacing Oxide−Oxo Cycle in the Presence of NO

$NO + FeO \leftrightarrows \mathbf{NO}\text{–}FeO$ (A)

$N_2O + \mathbf{NO}\text{–}FeO \leftrightarrows N_2O\text{–}\mathbf{NO}\text{–}FeO$ (B)

$N_2O\text{–}\mathbf{NO}\text{–}FeO \leftrightarrows \mathbf{NO_2}\text{–}FeO + N_2$ (C)

$N_2O + \mathbf{NO_2}\text{–}FeO \leftrightarrows N_2O\text{–}\mathbf{NO_2}\text{–}FeO$ (D)

$N_2O\text{–}\mathbf{NO_2}\text{–}FeO \leftrightarrows O_2\text{–}\mathbf{NO}\text{–}FeO + N_2$ (E)

$O_2\text{–}\mathbf{NO}\text{–}FeO \leftrightarrows \mathbf{NO}\text{–}FeO + O_2$ (F)

SCHEME 5: Nitrite−Nitrate Redox Cycle Replacing Oxide−Oxo Cycle in the Presence of NO

$2\,NO + O_2 \leftrightarrows 2\,NO_2$ (A)

$NO_2 + FeO \leftrightarrows \mathbf{NO_2}\text{–}FeO$ (B)

$N_2O + \mathbf{NO_2}\text{–}FeO \leftrightarrows N_2O\text{–}\mathbf{NO_2}\text{–}FeO$ (C)

$N_2O\text{–}\mathbf{NO_2}\text{–}FeO \leftrightarrows \mathbf{NO_3}\text{–}FeO + N_2$ (D)

$N_2O + \mathbf{NO_3}\text{–}FeO \leftrightarrows N_2O\text{–}\mathbf{NO_3}\text{–}FeO$ (E)

$N_2O\text{–}\mathbf{NO_3}\text{–}FeO \leftrightarrows O_2\text{–}\mathbf{NO_2}\text{–}FeO + N_2$ (F)

$O_2\text{–}\mathbf{NO_2}\text{–}FeO \leftrightarrows \mathbf{NO_2}\text{–}FeO + O_2$ (G)

TABLE 3: Calculated Overall Energy Changes for Several Redox Cycles

mechanistic reaction step	ΔE, kJ mol^{-1} naked cluster
Oxide−Oxo Redox Cycle (Scheme 1)	
$N_2O + FeO \rightarrow OFeO + N_2$	−119.9
$N_2O + OFeO \rightarrow FeO + O_2 + N_2$	10.9
Nitro−Nitrite Redox Cycle (Scheme 4)	
$(NO)FeO + N_2O \rightarrow (NO_2)FeO + N_2$	−147.7
$(NO_2)FeO + N_2O \rightarrow (NO)FeO + N_2 + O_2$	38.6
Nitrite−Nitrate Redox (Scheme 5)	
$NO_2-FeO + N_2O \rightarrow NO_3-FeO + N_2$	−144.8
$NO_3-FeO + N_2O \rightarrow NO_2-FeO + N_2 + O_2$	35.7
Alternate Nitrite−Nitrate Redox Cycle 1:	
$(NO_2)Fe(NO_2) + N_2O \rightarrow (NO_2)Fe(NO_3) + N_2$	−144.0
$(NO_2)Fe(NO_3) + N_2O \rightarrow (NO_2)Fe(NO_2) + N_2 + O_2$	34.9
Alternate Nitrite−Nitrate Redox Cycle 2:	
$(NO_2)Fe(NO_3) + N_2O \rightarrow (NO_3)Fe(NO_3) + N_2$	−147.6
$(NO_3)Fe(NO_3) + N_2O \rightarrow (NO_2)Fe(NO_3) + N_2 + O_2$	38.5
Alternate Nitrite−Nitrate Redox Cycle 3:	
$(NO_2)Fe(NO_2) + N_2O \rightarrow (NO_3)Fe(NO_2) + N_2$	−146.0
$(NO_3)Fe(NO_2) + N_2O \rightarrow (NO_2)Fe(NO_2) + N_2 + O_2$	37.0
Alternate Nitrite−Nitrate Redox Cycle 4:	
$(NO_3)Fe(NO_2) + N_2O \rightarrow (NO_3)Fe(NO_3) + N_2$	−145.5
$(NO_3)Fe(NO_3) + N_2O \rightarrow (NO_3)Fe(NO_2) + N_2 + O_2$	36.5

energies will differ from that observed in the absence of added NO (again consistent with experiment). These schemes would be consistent with the available spectroscopic evidence,[14,17,21,32] too.

Preliminary thermochemistry calculations (energies of stable intermediates, but not yet transition states) have been performed in Schemes 4 and 5. The results are presented in Table 3, where two observations are possible. First, the gross energetics of these cycles are comparable to those of the oxide−oxo pathway (Scheme 1, also included in Table 3). Second, it appears that when an iron cation has more than one ligand associated with it, the overall thermochemistry of redox cycles involving one of the ligands is largely independent of the identity of the other ligand.

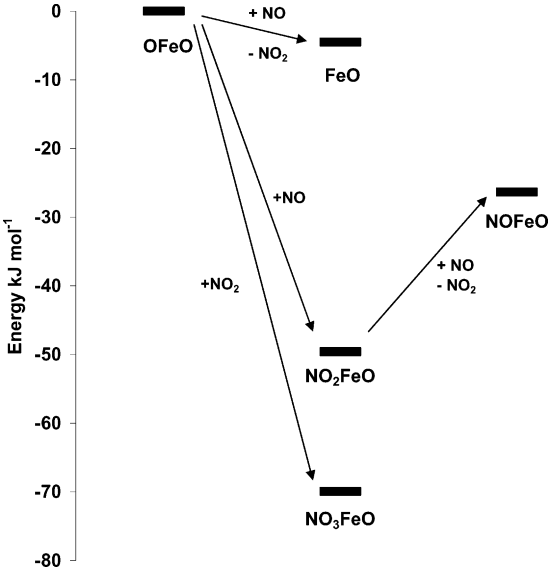

Figure 6. Energy changes calculated using the naked cluster model for the conversion of OFeO by NO/NO_2.

Finally, it was noted experimentally that only a small amount of NO needed to be added to cause a large increase in the rate, after which additional NO had little effect (Figure 4). In terms of the present discussion, this suggests that only a very small amount of NO needs to be added to effect a shift from OFeO as the most abundant surface intermediate (Scheme 1) to either FeO (Scheme 2 or 3), NOFeO (Scheme 4), NO_2FeO (Schemes 4 or 5), or NO_3FeO (Scheme 5). In this light, it is interesting to consider the energetics of formation of these new intermediates from OFeO and NO/NO_2. Figure 6 plots the calculated energy changes. It can be seen that all are favorable but to varying degrees. The energetic driving force is greatest for the formation of a nitrate. Such a nitrate species might function either as an oxygen storage site in Scheme 2 or as part of a redox couple as in Scheme 5.

Conclusions

The kinetics of N_2O decomposition have been studied over Fe/ZSM-5 catalysts with low aluminum content where it is expected that most of the exchanged cations exist as isolated species widely separated from other exchanged cations. The observed kinetic behavior is the same as that previously observed using Fe/ZSM-5 catalysts with larger iron loadings. Specifically, the reaction is first order in the partial pressure of N_2O. This is true if no additives are present, and it is also true when NO is added to the system. The addition of NO causes the rate of N_2O decomposition to increase by an order of magnitude or more. The increase in rate upon the addition of NO is accompanied by a decrease in the apparent preexponential factor and a decrease in the apparent activation energy, but the kinetics remain first order in N_2O. These observations indicate that extra sites adjacent to the catalytically active site are not essential to the promotional effect of added NO. In the absence of added NO, a pathway involving oxide−oxo redox cycles appears to be most consistent with available data, but when substoichiometric NO is added there are still several pathways that can describe available results to date.

Acknowledgment. This material is based upon work supported, in part, by the National Science Foundation under Award CTS-0099359. The use of facilities at the Center for Computational Research at the University at Buffalo, SUNY is also gratefully acknowledged.

References and Notes

(1) Delgass, W. N.; Garten, R. L.; Boudart, M. *J. Phys. Chem.* **1969**, *73*, 2970.
(2) Garten, R. L.; Delgass, W. N.; Boudart, M. *J. Catal.* **1970**, *18*, 90.
(3) Ione, K. G.; Bobrov, N. N.; Boreskov, K. G.; Vostrikova, L. A. *Dokl. Akad. Nauk SSSR* **1973**, *210*, 388.
(4) Kubo, T.; Tominaga, H.; Kunugi, T. *Bull. Chem. Soc. Jpn.* **1973**, *46*, 3549.
(5) Leglise, J.; Petunchi, J. O.; Hall, W. K. *J. Catal.* **1984**, *86*, 392.
(6) Aparicio, L. M.; Dumesic, J. A. *J. Mol. Catal.* **1989**, *49*, 205.
(7) Panov, G. I.; Sheveleva, G. A.; Kharitonov, A. S.; Romannikov, V. N.; Vostrikova, L. A. *Appl. Catal., A* **1992**, *82*, 31.
(8) Panov, G. I.; Sobolev, V. I.; Kharitonov, A. S. *J. Mol. Catal.* **1990**, *61*, 85.
(9) Panov, G. I.; Uriarte, A. K.; Sobolev, V. I. *Catal. Today* **1998**, *41*, 365.
(10) Kapteijn, F.; Marbán, G.; Rodriguez-Mirasol, J.; Molijn, J. A. *J. Catal.* **1997**, *167*, 256.
(11) Kapteijn, F.; Rodriguez-Mirasol, J.; Moulijn, J. A. *Appl. Catal., B* **1996**, *9*, 25.
(12) Sang, C.; Lund, C. R. F. *Catal. Lett.* **2001**, *73*, 73.
(13) Ryder, J. A.; Chakraborty, A. K.; Bell, A. T. *J. Phys. Chem. B* **2002**, *106*, 7059.
(14) Wood, B. R.; Reimer, J. A.; Bell, A. T. *J. Catal.* **2002**, *209*, 151.
(15) Perez-Ramirez, J.; Kapteijn, F.; Mul, G.; Moulijn, J. A. *J. Catal.* **2002**, *208*, 211.
(16) Chen, H. Y.; El-Malki, E. M.; Sachtler, W. M. H. *J. Mol. Catal.* **2000**, *162*, 159.
(17) Chen, H. Y.; Sachtler, W. M. H. *Catal. Today* **1998**, *42*, 73.
(18) Chen, H. Y.; Voskoboinikov, T.; Sachtler, W. M. H. *Catal. Today* **1999**, *54*, 483.
(19) Chen, H. Y.; Wang, X.; Sachtler, W. M. H. *Appl. Catal., A* **2000**, *194*−*195*, 159.
(20) Chen, H.-Y.; Sachtler, W. M. H. *Catal. Lett* **1998**, *50*, 125.
(21) Chen, H.-Y.; Voskoboinikov, T.; Sachtler, W. M. H. *J. Catal.* **1998**, *180*, 171.
(22) Chen, H.-Y.; Voskoboinikov, T.; Sachtler, W. M. H. *J. Catal.* **1999**, *186*, 91.
(23) Chen, H.-Y.; Wang, X.; Sachtler, W. M. H. *Phys. Chem. Chem. Phys.* **2000**, *2*, 3083.
(24) Sang, C. S.; Lund, C. R. F. *Catal. Lett.* **2000**, *70*, 165.
(25) *Athena Visual Workbench*, 7.0 ed.; Stewart and Associates, Inc.: Madison, WI, 1997.
(26) *Jaguar*, 3.5, 4.0, 4.1 ed.; Schrodinger, Inc.: Portland, OR, 1998.
(27) Yakovlev, A. L.; Zhidomirov, G. M.; van Santen, R. A. *J. Phys. Chem. B* **2001**, *105*, 12297.
(28) Olson, D. H.; Kokotallo, G. T.; Lawton, S. L.; Meier, W. M. *J. Phys. Chem.* **1981**, *85*, 2238.
(29) Moden, B.; Da Costa, P.; Lee, D. K.; Iglesia, E. *J. Phys. Chem. B* **2002**, *106*, 9633.
(30) Moden, B.; Da Costa, P.; Fonfe, B.; Lee, D. K.; Iglesia, E. *J. Catal.* **2002**, *209*, 75.
(31) Da Costa, P.; Moden, B.; Meitzner, G. D.; Lee, D. K.; Iglesia, E. *Phys. Chem. Chem. Phys.* **2002**, *4*, 4590.
(32) Voskoboinikov, T. V.; Chen, H. Y.; Sachtler, W. M. H. *Appl. Catal., B* **1998**, *19*, 279.